Polar rain gradients and field-aligned polar cap potentials

D. H. Fairfield,[1] S. Wing,[2] P. T. Newell,[2] J. M. Ruohoniemi,[2,3] J. T. Gosling,[4] and R. M. Skoug[5]

Received 29 May 2008; accepted 24 July 2008; published 7 October 2008.

[1] ACE SWEPAM measurements of solar wind field-aligned electrons have been compared with simultaneous measurements of polar rain electrons precipitating over the polar cap and detected by DMSP spacecraft. Such comparisons allow investigation of cross-polar-cap gradients in the intensity of otherwise-steady polar rain. The generally good agreement of the distribution functions, f, from the two data sources confirms that direct entry of solar electrons along open field lines is indeed the cause of polar rain. The agreement between the data sets is typically best on the side of the polar cap with most intense polar rain but the DMSP f's in less intense regions can be brought into agreement with ACE measurements by shifting all energies by a fixed amounts that range from tens to several hundred eV. In most cases these shifts are positive which implies that field-aligned potentials of these amounts exist on polar cap field lines which tend to retard the entry of electrons and produce the observed gradients. These retarding potentials undoubtedly appear in order to prevent the entry of low-energy electrons and maintain charge quasi-neutrality that would otherwise be violated since most tailward flowing magnetosheath ions are unable to follow polar rain electrons down to the polar cap. In more limited regions near the boundary of the polar cap there is sometimes evidence for field-aligned potentials of the opposite sign that accelerate polar rain electrons. A solar electron burst is also studied and it is concluded that electrons from such bursts can enter the magnetotail and precipitate in the same manner as polar rain.

Citation: Fairfield, D. H., S. Wing, P. T. Newell, J. M. Ruohoniemi, J. T. Gosling, and R. M. Skoug (2008), Polar rain gradients and field-aligned polar cap potentials, *J. Geophys. Res.*, *113*, A10203, doi:10.1029/2008JA013437.

1. Introduction

[2] Uniform precipitation of few-hundred-eV electrons over Earth's polar caps has been known as polar rain since its discovery in 1974 [*Winningham and Heikkila*, 1974]. This precipitation is generally more intense over one polar cap than the other, with the ''preferred'' hemisphere depending on the sunward or antisunward orientation of the IMF (Interplanetary Magnetic Field, i.e., the negative or positive interplanetary sector structure) [e.g., see *Shirai et al.*, 1998, and references therein]. *Fairfield and Scudder* [1985] argued that that the source of polar rain is field-aligned electrons of the solar wind "strahl" that carry a heat flux outward from the Sun. Those electrons following field lines that connect to the magnetotail can move all the way to low altitudes over the polar cap. (It should be appreciated that when solar wind electrons move along field lines and conserve their first adiabatic invariant, $\mu = B/V_\perp^2$, where B is the magnetic field strength and $V_\perp$ the velocity component perpendicular to the field, only those electrons within about 1 degree of field alignment reach the DMSP (Defense Meteorology Satellite Program) altitude of 835 km; all larger pitch angles mirror in the increasingly stronger tail fields at higher altitudes.) Positive sector field lines pointing outward from the Sun connect to the northern tail lobe so that the outward moving strahl electrons precipitate in the north. In such a positive sector the southern hemisphere is connected to IMF field lines leading to the outer heliosphere so only weaker fluxes in the antistrahl direction precipitate in the south. In negative sectors everything reverses and the southern hemisphere becomes the preferred hemisphere.

[3] A number of studies tend to confirm the Fairfield/Scudder scenario. *Greenspan et al.* [1986] compared electrons at ISEE 1 at approximately 20 Re in the tail with those at the DMSP spacecraft at low altitudes over the polar cap. (Louisville's theorem dictates that the distribution functions can be directly compared at all locations along the field line.) *Baker et al.* [1986] detected bidirectional field-aligned electrons on ISEE 3 in the distant tail; the outgoing electrons are explained as incoming electrons that had mirrored in the strong magnetic fields at lower altitudes and returned to the spacecraft. Motion of the tail allowed them to see north and south lobes in rapid succession where

[1]Space Weather Laboratory, NASA Goddard Space Flight Center, Greenbelt, Maryland, USA.
[2]Johns Hopkins University Applied Physics Laboratory, Laurel, Maryland, USA.
[3]Now at Bradley Department of Electrical and Computer Engineering, Virginia Polytechnic and State University, Blacksburg, Virginia, USA.
[4]Laboratory for Atmospheric and Space Physics, University of Colorado, Boulder, Colorado, USA.
[5]Los Alamos National Laboratory, Los Alamos, New Mexico, USA.

Copyright 2008 by the American Geophysical Union.
0148-0227/08/2008JA013437

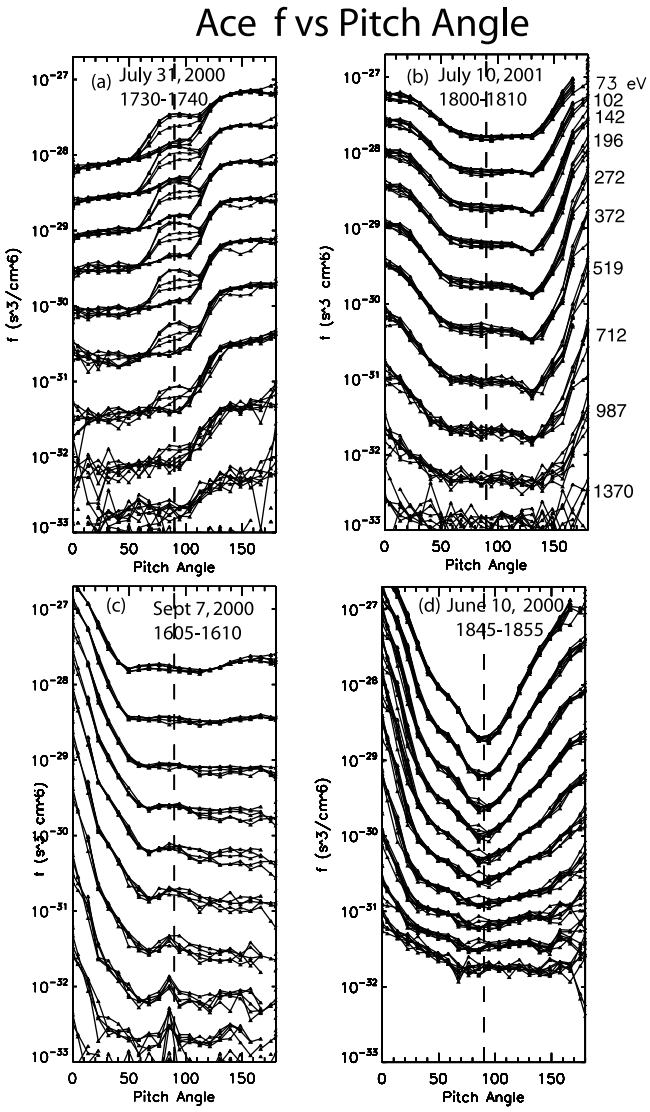

Figure 1. Four plots of ACE electron distribution functions plotted versus pitch angle. The largest electron fluxes are moving antisunward and appear at either 0° or 180° depending on the direction of the IMF.

they could see the presence/absence of the electrons associated with the preferred/unpreferred polar cap. *Baker et al.* [1987] found generally favorable comparisons between ISEE 3 electron flux measurements and DMSP flux measurements at low altitudes. *Shirai et al.* [1998] studied Geotail electrons near the tail boundary and they could sometimes see the bidirectional electrons rotate with the field as the spacecraft crossed into the magnetotail, presumably through a rotational discontinuity. In other crossings with abrupt magnetic field changes (undoubtedly tangential discontinuities), they saw only the unidirectional strahl electrons in the magnetosheath adjacent to the bidirectional electrons in the lobe. *Gosling et al.* [1986] looked at unusual cases where polar rain of equal intensity was present over both polar caps. They found bidirectional solar wind heat flux present in these cases that could explain their observations.

[4] Other observations presented features not readily explained by the simple model of direct electron access to the polar cap. *Meng et al.* [1977] presented evidence for a dawn/dusk intensity gradient across the polar cap whose direction depended on the IMF. When the interplanetary B_y was positive (negative), the northern hemisphere fluxes tended to be higher near dawn (dusk). Higher fluxes were also noted to be associated with stronger polar cap convection electric fields. A statistical study of the polar rain [*Gussenhoven et al.*, 1984] used one year's worth of DMSP passes to construct polar cap maps of average polar rain flux intensity and average energy. These maps revealed a large day/night gradient in polar rain flux with high fluxes associated with low average energies.

[5] *Wing et al.* [1996] extended a theoretical model of *Onsager et al.* [1993] in order to explain the entry of magnetosheath electrons into the dayside ionosphere. Realizing that higher velocity magnetosheath electrons would have easier access to the polar cap via open field lines than the tailward flowing ions, they introduced a potential that would prevent the entry of low-energy electrons that would otherwise create a charge imbalance. With potentials not larger than a few hundred eV they were able to explain the observations rather well.

[6] As solar coronal electrons follow field lines out to 1 AU, they tend to move adiabatically and become more field-aligned as the magnetic field strength decreases. This alignment will occur, however, only as long as coulomb collisions or any other scattering mechanism do not broaden the pitch angle distribution. Indeed *Ogilvie et al.* [2000], in studying 9 intervals with very low solar wind density, found strahl pitch angle distributions with widths less than their 3.5 degree instrumental threshold. For higher densities and more typical conditions the distributions can have widths of several tens of degrees [e.g., *Pagel et al.*, 2007, and references therein]. Collisional scattering can only partially explain such broad distributions and some other unknown broadening mechanism must also be active.

[7] In the present paper we report results of a direct, detailed comparison of field-aligned solar wind electrons measured by the SWEPAM (Solar Wind Electron Proton Alpha Monitor) experiment on the ACE spacecraft with the precipitating electrons measured simultaneously by several DMSP spacecraft at low altitudes over the polar cap. Similar day to day changes in the distribution functions at both locations confirm the direct entry mechanism. The primary objective, however, is to study the polar cap gradients by comparing the relatively steady solar wind electrons with the spatially varying DMSP electrons. These ACE/DMSP differences are interpreted as evidence for field-aligned potentials that can explain the polar cap gradients.

2. Observing Spacecraft

[8] Solar wind electrons from 73 eV to 1.37 keV have been continually measured by the ACE SWEPAM electrostatic analyzer since the August 1997 launch [*McComas et al.*, 1998]. The ACE magnetic field measurements [*Smith et al.*, 1998] are used to sort the electron data into 20, 9° pitch angle bins for successive 64 s intervals. In this paper we will be concerned primarily with the 2 bins containing those particles aligned most parallel and antiparallel to the field since those are the electrons that are able to follow field lines down to low altitudes. Four examples are shown in Figure 1 where electron distribution functions, f, are plotted versus pitch angle. When the slope of the pitch angle

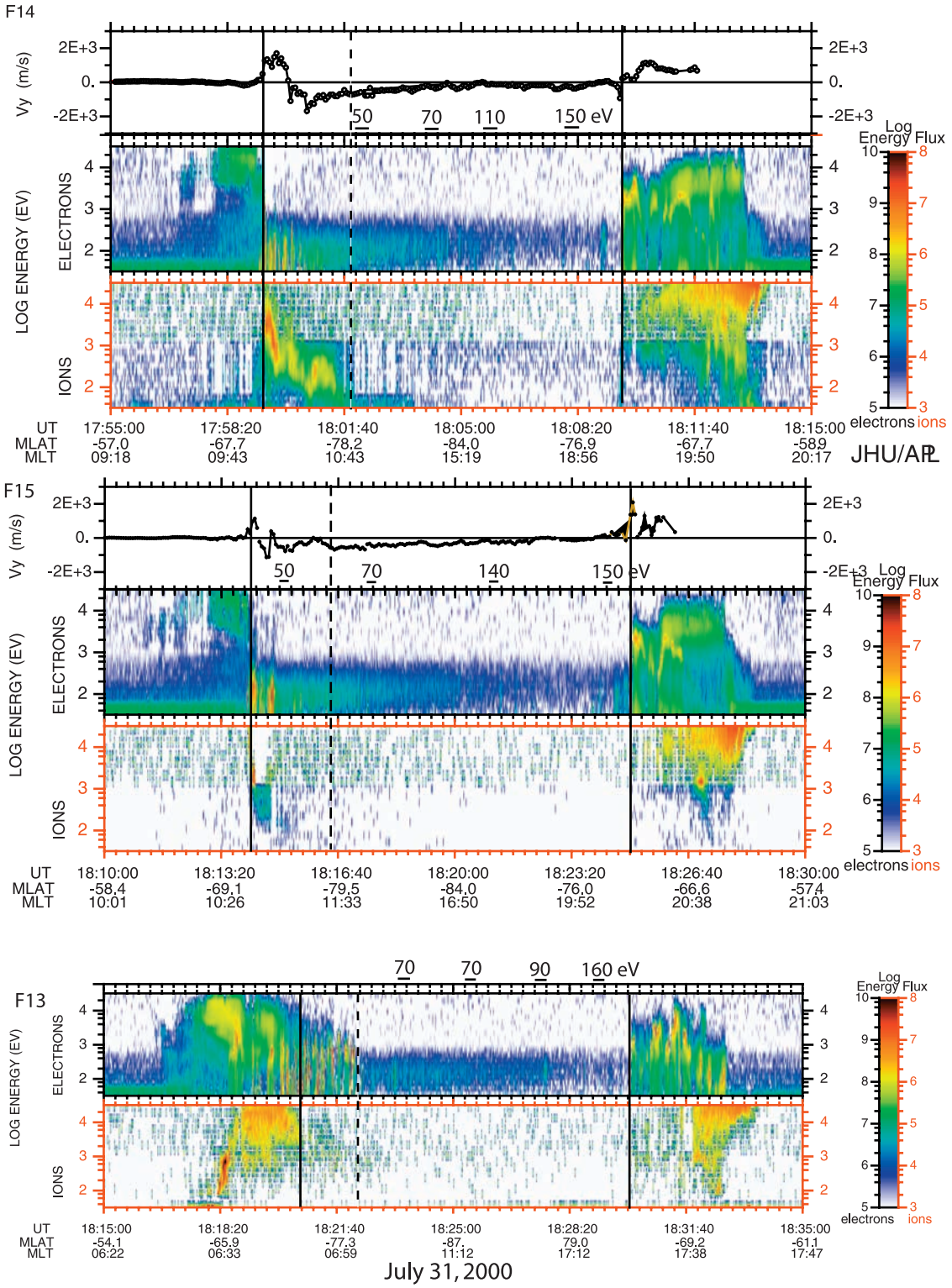

Figure 2. Three passes of different DMSP spacecraft over the southern polar cap on 31 July 2000. Data from each pass include the velocity component V_y perpendicular to the spacecraft trajectory followed by spectrograms representing precipitating electrons and ions. Gradients in the precipitating electron intensity are apparent. Field-aligned potentials and their points of determination are indicated by numbers above the associated bars (see text and Figure 3).

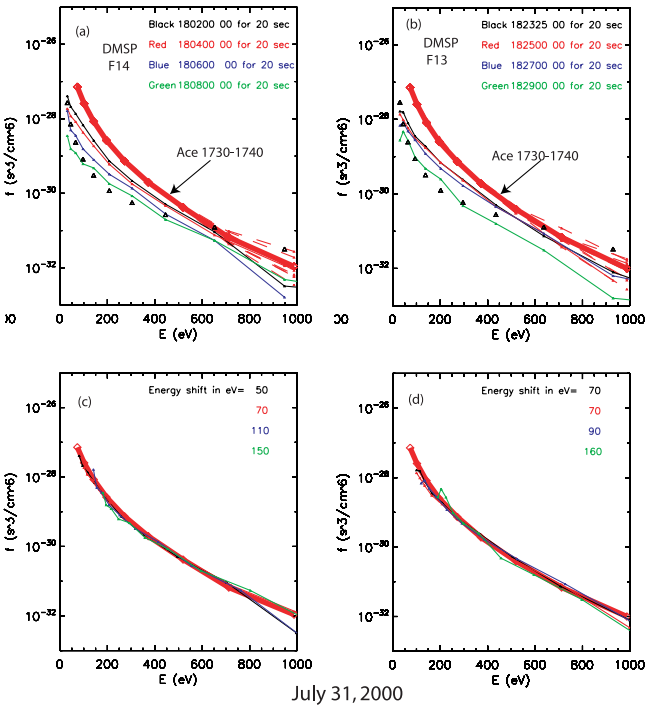

Figure 3. (a) ACE and DMSP F14 electron distribution functions plotted versus energy for the first pass shown in Figure 2. ACE data at 180° are shown by the heavy red trace and DMSP data from four different 20 s intervals are shown by the four thinner traces. (c) Same data shifted to the right to best overlay the ACE data. The shifts are interpreted as field-aligned potentials that have decelerated the precipitating electrons and their magnitudes are indicated here and in Figure 2. (b) and (d) Similar data from the F13 pass in Figure 2.

distribution is steep as near 0° on 7 September 2000, the most field-aligned f value is probably higher than the samples obtained from measurements throughout the 0–9° bin (which is plotted at the central angle of 4.5°). For this reason the two most field-aligned points are used to extrapolate to a zero degree value which is normally slightly higher than the 9° point. This procedure seems to produce somewhat better agreement with the DMSP data but does not significantly effect the conclusions in the paper.

[9] For many years a series of DMSP spacecraft have orbited Earth in circular polar orbits near 835 km altitude. These spacecraft have periods of about 100 min and carry electrostatic analyzers that measure precipitating ions and electrons with one second time resolution. The electrons energies range from 30 eV to 30 keV in 19 logarithmically spaced buckets. In recent years these spacecraft have also carried ion drift meters and retarding potential analyzers to measure plasma velocity along and perpendicular to the orbital motion [*Rich and Hairston*, 1994]. The perpendicular velocity has greater accuracy and we will utilize only this V_y velocity which is readily available at 4 s time resolution.

3. Observations

[10] To study the gradient in polar rain precipitation and its relation to the solar wind electrons, 4 d (10 June, 31 July, 7 September 2000 and 10 July 2001) were selected on the basis of their extended intervals of southward IMF which invariably leads to an open polar cap and steady polar rain. Online plots of ACE SWEPAM electrons http://swepam-pub.lanl.gov/plots/ were also scanned to assure the presence of field-aligned electrons with relatively few time variations. Electron distribution functions were used for these 4 d along with 22 and 24 October 2003 that were of interest because they bracket a day that was of interest for its very northward IMF. Examples of pitch angle distributions on 4 different days illustrate cases from a toward sector with a maximum at 180° and an away sector with maximum at 0° in Figures 1a and 1c, respectively. Figures 1b and 1d show maxima at both 0° and 180° which indicates closed interplanetary field lines with both ends leading back to the Sun.

[11] On 31 July 2000, 3 different DMSP spacecraft measured clear polar rain as they passed over the southern polar cap between 1800 and 1830 UT during a toward IMF sector with negative B_y. Figure 2 shows spectrograms for electrons and ions at these spacecraft, F14, F15 and F13. Above the spectrograms are the DMSP velocity components perpendicular to the spacecraft trajectory. Magnetic latitude and magnetic local time are tabulated below the spectrograms of each spacecraft. Solid vertical lines indicate the high-latitude boundaries of precipitating magnetospheric energetic electrons. Field lines poleward of this boundary are mostly open field lines. The region between the solid line and the dashed lines are probably low-latitude boundary layer and may be open or closed. Poleward of the dashed vertical lines is polar rain with gradients that are readily apparent. Greater polar rain intensities are present on the dawn side of the polar cap in agreement with *Meng et al.* [1977] for $-B_y$ IMF conditions.

[12] Figure 3 shows electron distribution functions plotted versus energy for electrons precipitating at DMSP F14 on the left and F15 on the right. The four thin colored lines correspond to the averages for four 20 s periods as indicated by the start times in the top panels. Black triangles indicate the one count level for DMSP data. The red diamonds connected by a heavy red line display ACE data averaged for the interval 1730–1740. The ACE time interval precedes the DMSP interval by some 40 min to allow for the ACE field lines to convect to Earth. Although the electrons are moving outward from the Sun very rapidly, the electrons on any field line are presumed to reflect a relatively steady source near the Sun [*Gosling et al.*, 2004b]. The time shift is introduced to allow the relevant field lines to convect to Earth. In this 31 July case the electrons are very steady so the time delay is not important, but on other days the ACE electrons exhibit time variations and choosing the appropriate delay is more important. The two DMSP passes had quite similar trajectories and were only separated in time by about 15 min. The similarities of intensities at the two spacecraft imply good intercalibration at the two DMSP spacecraft and their traces have a similar relationship to ACE. In the bottom plots the DMSP traces have been shifted in energy by the amounts indicated on the plots to best make them agree with ACE. The excellent agreement here and on other plots will be interpreted as evidence for field-aligned potentials whose spatial variation creates the polar rain gradient. A similar plot for F13 (not shown) reveals similar potentials when its traces are aligned. These

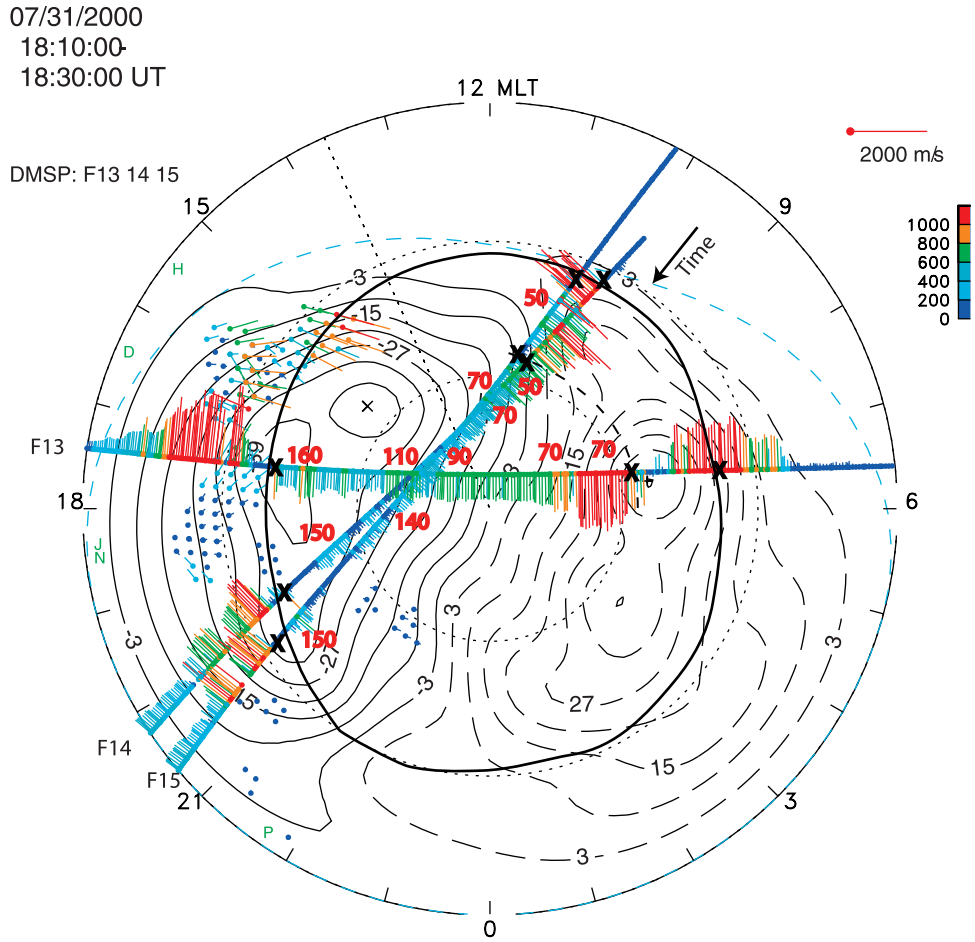

Figure 4. DMSP Trajectories of the three polar cap passes of Figure 1 are shown in a view of the southern polar cap looking down through the Earth. V_y velocities are shown perpendicular to the trajectories. These data along with SuperDARN velocity vectors associated with the dots have been used to calculate the polar cap potentials represented by the underlying thin dashed lines. Field-aligned potential from Figures 2 and 3 are indicated by large red numbers at their positions of determination. A heavy black line is drawn through the heavy crosses representing the high-latitude boundary of energetic precipitation represented by vertical lines in Figure 2.

potentials and their spatial locations are indicated in Figure 2 by the bars and associated numbers over the electron spectrograms. Note that the positive shifts needed to restore the agreement with ACE imply that the precipitating electrons have been decelerated by the field-aligned potential.

[13] Figure 4 summarizes the above results and places them in context. This view of the southern polar cap looking through the Earth from the north shows the trajectories of the three DMSP spacecraft with the color-coded, measured velocities perpendicular to the trajectory. The black X's mark the high-latitude boundary of precipitating energetic electrons indicated by the solid vertical lines in Figure 2; the solid heavy line is sketched in to represent a possible polar cap boundary based on these points. The underlying contours are electric potentials (equivalently ionospheric flow lines) calculated from SuperDARN radar data [*Chisham et al.*, 2007] along with the DMSP velocity measurements using the potential fitting technique of *Ruohoniemi and Baker* [1998] and *Shepherd and Ruohoniemi* [2000]. The available SuperDARN line of sight velocity measurements are overplotted.

[14] The black labels indicate these perpendicular potentials in keV. The heavy red numbers are the field-aligned potentials from Figure 3 plus those for F13. These field-aligned potentials range from 50 eV near 1000 LT to about 160 eV on the dusk side and delineate a gradient consistent with that reported by *Meng et al.* [1977]. Note that the dusk side polar cap boundaries are well defined by the low-latitude termination of antisolar flow, whereas on the dawn side there is a flow reversal poleward of the solid line. A higher-latitude boundary indicated by the dashed lines in Figure 2 denotes the low-latitude boundary of unequivocal polar rain. (It is generally accepted that the regions designated mantle and polar rain are both on open field lines with the distinguishing feature between the two being that a measureable fraction of hot ions in the downtail plasma flow move opposite to this bulk velocity, reach DMSP altitude and create the mantle classification [*Newell et al.*, 1991c]. Since we are concerned only with electrons in this paper, we will not distinguish between these two categories.) The region between these dawn side lines is classified as LLBL, mantle or BPS in the automated scheme of *Newell*

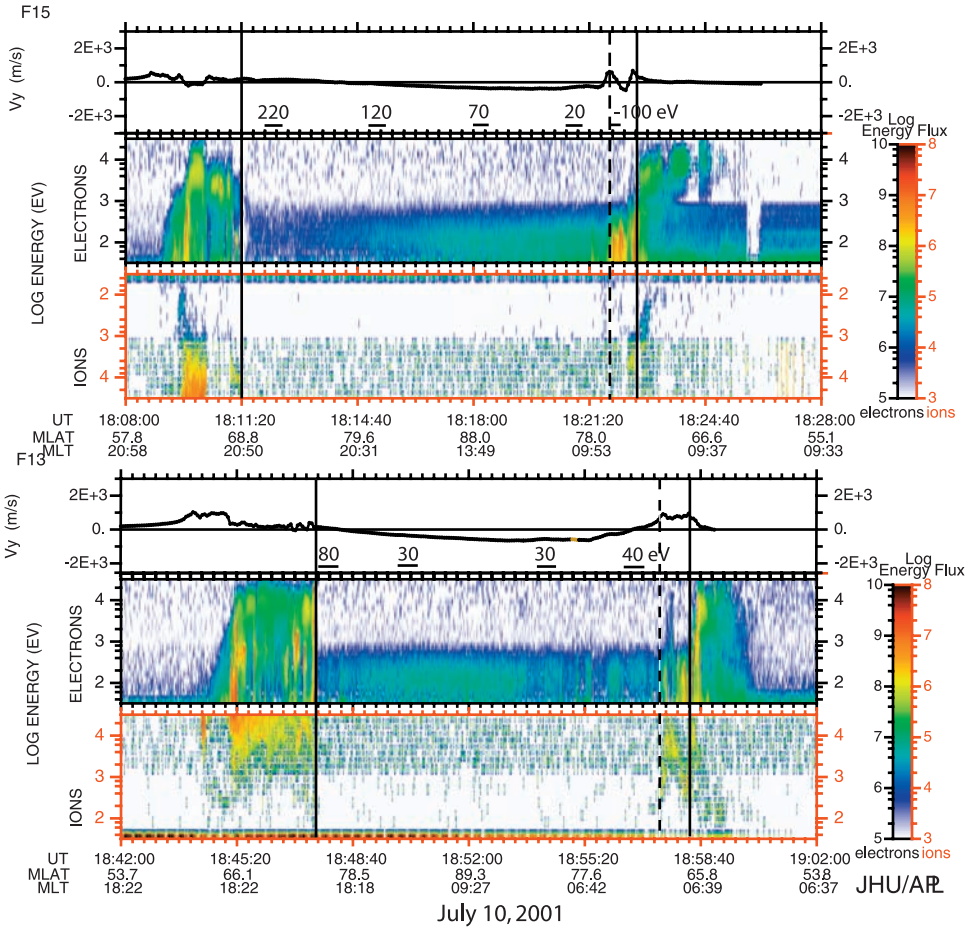

Figure 5. Two northern hemisphere passes of DMSP F15 and F13 on 10 July 2001 in the same format as Figure 2.

et al. [1991a], all of which may be on open field lines. The convection reversals were often found to be in the LLBL by *Newell et al.* [1991b].

[15] A second example during a period of very southward IMF with only a small negative B_y comes from 10 July 2001 when three spacecraft crossed the northern polar cap between 1810 and 1905. The F15 and F13 passes are shown in Figure 5 in the same format as Figure 2. F15 moved across the polar cap from 2050 LT to 0950 MLT and detected what is undoubtedly the day/night gradient discussed by *Gussenhoven et al.* [1984]. F13 moved across the polar cap from 1820 to 0640 MLT and observed little dawn/dusk asymmetry, probably because of the almost directly southward IMF. F14 has a data gap near the pole but it detected polar rain and dusk and dawn boundary crossings near 2025 and 0840 MLT. Figure 6 compares the electron distribution functions at DMSP and ACE, with the heavy black trace representing data at 0° pitch angle that enters the northern hemisphere. The 4 thin lines again represent DMSP data at 4 locations across the polar cap and in the bottom panels these traces again overlay ACE data when shifted by the amounts indicated. Figure 7 again shows the polar view of the three spacecraft. The largest decelerating potentials are seen on the night side by both F14 and F15.

[16] Another feature apparent in Figure 5 is the intense low-energy electron precipitation present detected by F15 near dawn at 1822 10 s UT. The source of these electrons is not clear. When their distribution functions are compared with ACE they are larger, but they can be shifted to the left to achieve rather good agreement with ACE, suggesting an acceleration process. This event occurs in the morning and is probably related to the cusp or its longitudinal extension. It is also possible that the higher intensities are due to higher densities of the subsolar magnetosheath and scattering into the loss cone.

[17] A third example comes from 24 October 2003 between 1100 and 1500 UT when the IMF was very steady and southward with a negative B_y component. Three consecutive passes of F13 over the northern polar cap are shown in Figure 8 in the same format as Figures 2 and 5 with the corresponding distribution functions in Figure 9. The expected gradient for negative IMF B_y in the northern hemisphere is exhibited by the weak fluxes during early morning hours at 1307 and 1447 UT. The third pass near 0930 LT (1124 UT) does not show a decrease at its more dayside location. Near the three dusk crossings of the polar cap boundary in Figure 8 (near 1114, 1254 and 1436), there is a gradual enhancement in the electron flux on approaching the dusk boundary from higher latitudes. The gradual nature of this increase suggests that these enhancements may be due to acceleration of polar rain electrons. This idea is supported by the distribution functions shown in Figure 9

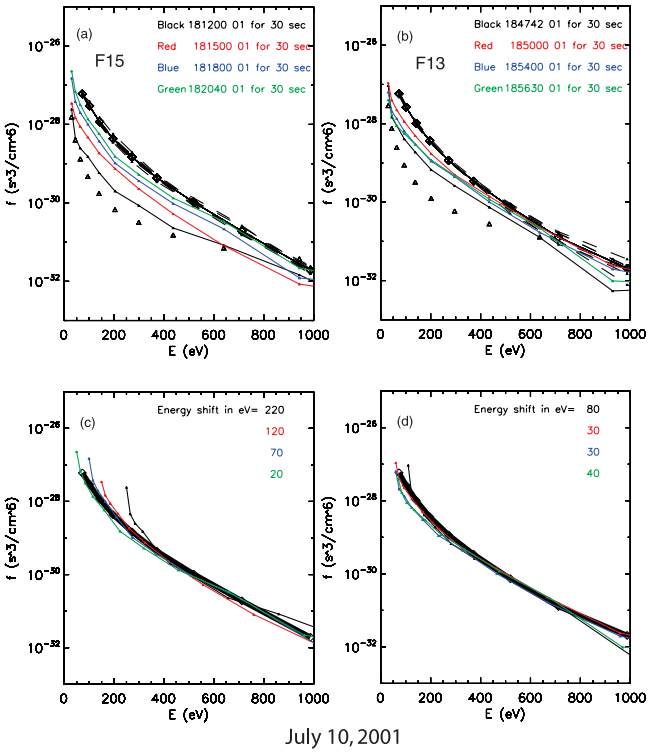

Figure 6. ACE and DMSP distribution functions in the same format as Figure 3. ACE data are represented by the heavy black trace in this northern hemisphere example. Both F15 and F13 can be aligned with ACE with a positive shift in energy.

for the first two passes where the thin black traces in Figures 9a and 9b correspond to the enhanced flux regions and are seen to be larger than the ACE values. Figures 9c and 9d show how negative shifts of these DMSP traces, by 80 and 450 eV respectively, produce very good agreement with ACE. The lack of significant F13 fluxes below about 600 eV at 1254 35 s suggests that ACE electrons below about 150 eV did not pass through the region where higher energies were accelerated. As in earlier examples, the other intervals across the polar cap can be aligned with ACE with positive shifts. The third F13 pass not shown in Figure 9 shows equally good agreement. Three F15 passes during this interval cross dusk at later local times and do not show the pre-dusk flux enhancements seen by F13 at earlier local times. The F15 locations and their calculated potentials are shown in Figure 10 which summarizes the results of the previous two figures including the negative (accelerating) potentials in the pre-noon and dusk regions. The SuperDARN velocity data here have been averaged (within fixed MLT-mlat bins) over 5 h of UT. This makes it possible to utilize multiple passes of the DMSP satellites. The SuperDARN data have been averaged within 10 deg azimuth bins and resolved statistical model vectors are also depicted. The most deceleration is seen at dawn as is typical for negative IMF B_y.

4. Solar Electron Event

[18] In addition to the relatively steady solar heat flux that produces polar rain, the Sun often emits bursts of electrons at energies that can range from ~100 eV to hundreds of keV [*Lin*, 1985]. Such burst have sudden onsets and slower decays that display energy dispersion, with higher energies arriving at 1 AU before lower energies [e.g., *Gosling et al.*, 2003, and references therein]. Many energetic solar electron bursts do not extend down to energies below 1 keV in detectable numbers; on the other hand, many low-energy bursts are not observed at energies greater than 20 keV [*Gosling et al.*, 2003, 2004a]. Such observations have been interpreted as due to both varying locations of the source region and propagation conditions between Sun and Earth [*Gosling et al.*, 2003, 2004a; *Wang et al.*, 2006]. Lower-energy events tend to be better associated with type 3 radio bursts whereas higher-energy events are more apt to be associated with solar flares and coronal mass ejections (CMEs).

[19] On 10 June 2000 the ACE SWEPAM experiment detected a low-energy electron burst beginning at ~1730 UT at 1.37 keV, the ACE EPAM (Electron Proton Alpha Monitor) experiment detected a 3-order-of-magnitude increase in >35 keV electrons beginning at ~1710 UT, and DMSP detected unusually energetic electrons over the north polar cap as we describe below. Energetic electrons from solar electron events have long been known to enter the magnetotail and in fact were early evidence that tail field lines were connected to the IMF [*Lin and Anderson*, 1966]. More recently, *Anderson et al.* [2000] used Polar observations to detect X-ray emissions over the polar cap that were associated with >10 keV precipitating solar electrons measured with DMSP. To our knowledge, however, the precipitation of solar electron bursts over the polar cap at energies <10 keV has not been previously reported.

[20] Figure 11a shows SWEPAM fluxes at $22 \pm 4.5°$ pitch angle and various energies on 10 June 2000. This particular pitch angle is used because low counting statistics at smaller pitch angles preclude observation of the increase at 1730 that is marked with a vertical dashed line in Figure 11a. Figure 11b shows data from the Wind Waves experiment which reveal three type 3 radio bursts at 1527, 1549 and 1656 UT that are potentially associated with the electron burst. (It happens that the Wind spacecraft was at perigee in the magnetosphere at this time and intense auroral kilometric radiation around several hundred kHz obscured the decreasing frequencies with time that are typically associated with type 3 events.) *Gopalswamy et al.* [2001] discuss the 1656 event, its association with a M5.2 solar flare, and an interaction of coronal mass ejections. The high-energy event detected by EPAM was apparently associated with the flare, the CME, and the 1656 radio burst since a 35 keV field-aligned electron can travel 1 AU in about 23 min. This time interval is consistent with the observed arrival time and with electrons being accelerated near the time of the flare and/or CME and prior to the 1656 type 3 event [*Wang et al.*, 2006].

[21] A 1.37 keV electron takes ~1.9 h to travel 1 AU so the low-energy electron increase at 1730 in Figure 11a clearly cannot be associated with the large 1656 event some 19 min earlier. However, the 1730 onset follows the 1527 and 1549 type 3 radio bursts by 2.0 and 1.7 h respectively which gives the highest-energy SWEPAM electrons time to arrive if they are generated near the time of the weak 1527 burst or perhaps slightly prior to the 1549 type 3 radio burst.

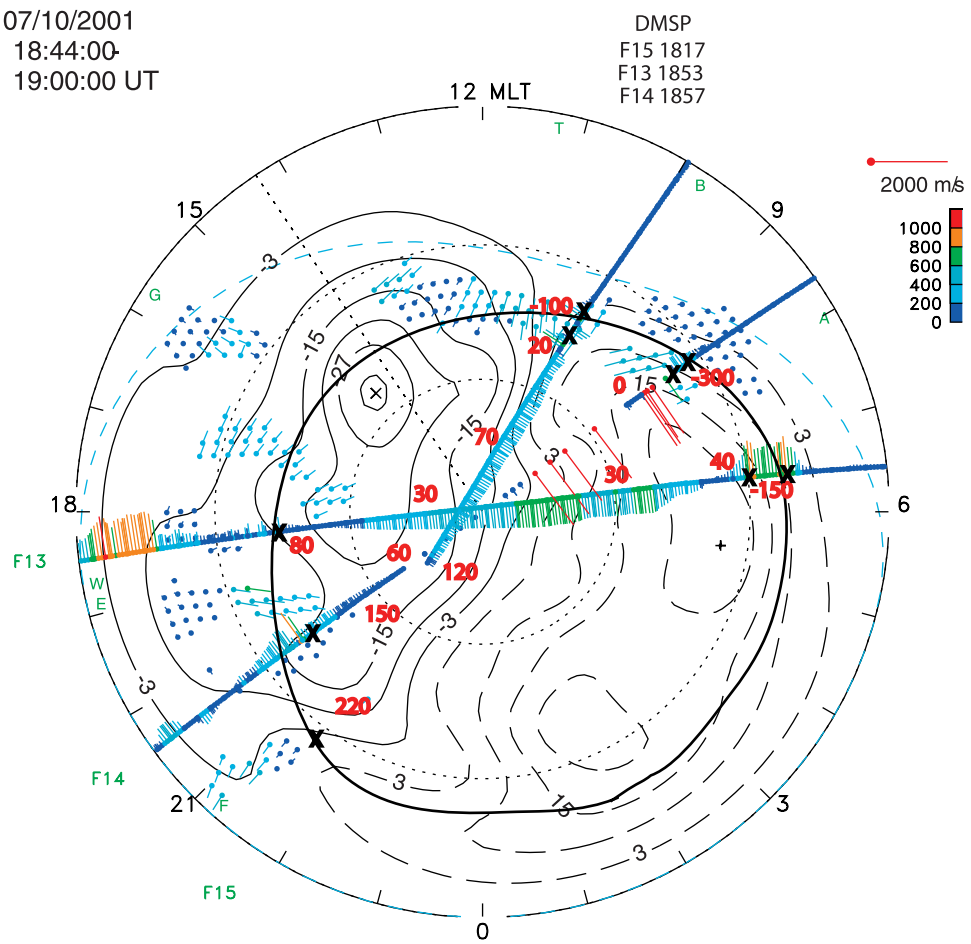

Figure 7. A view of the northern polar cap on 10 July 2001 in the same format as Figure 4. The highest potentials occur at night and evening locations.

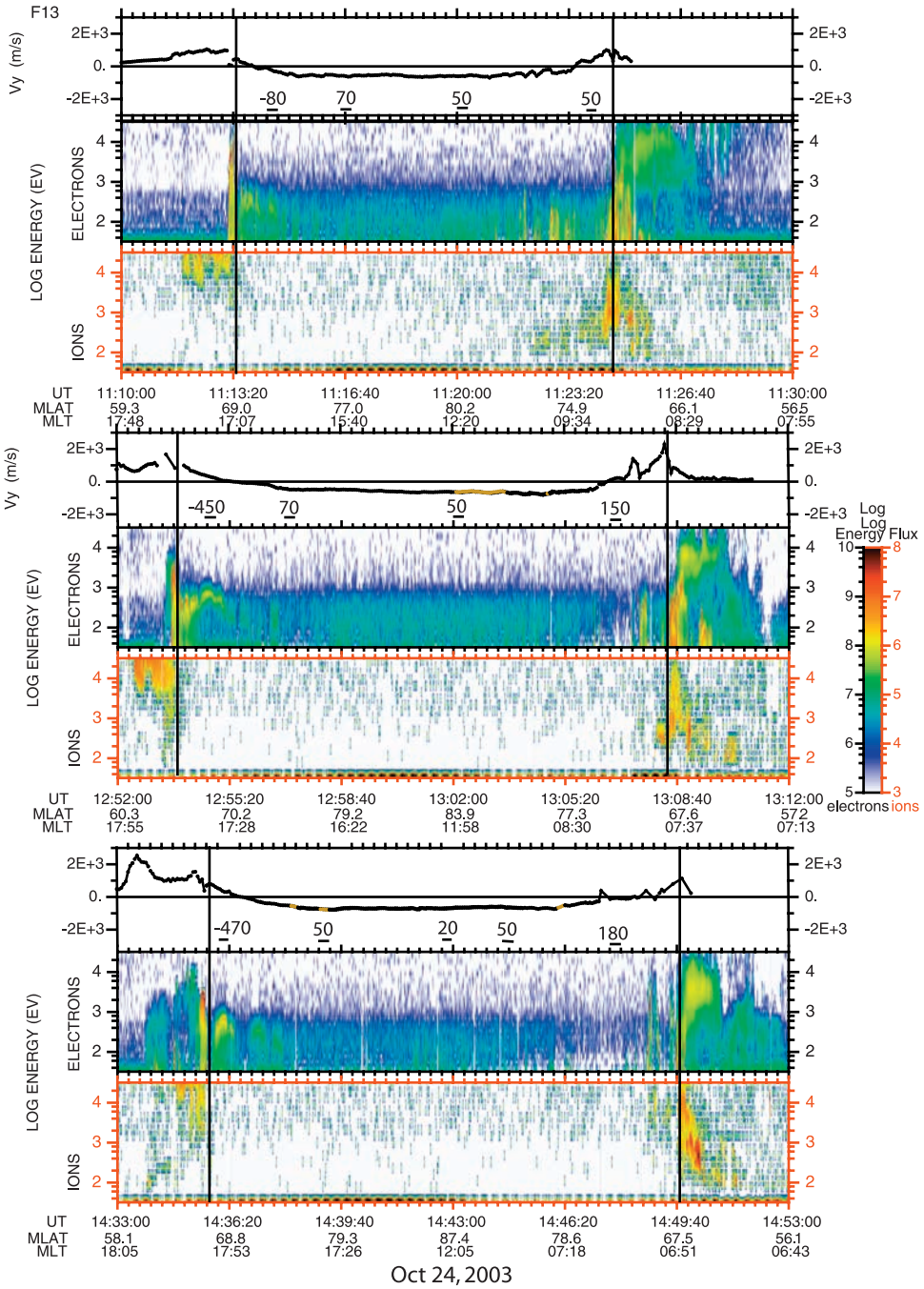

Figure 8. Three consecutive passes of F13 over the northern polar cap during an interval of steady southward IMF on 24 October 2003. The format is the same as Figures 2 and 5. Note that the polar rain extends to higher energies on this day. Enhanced fluxes near dusk suggest accelerating potentials.

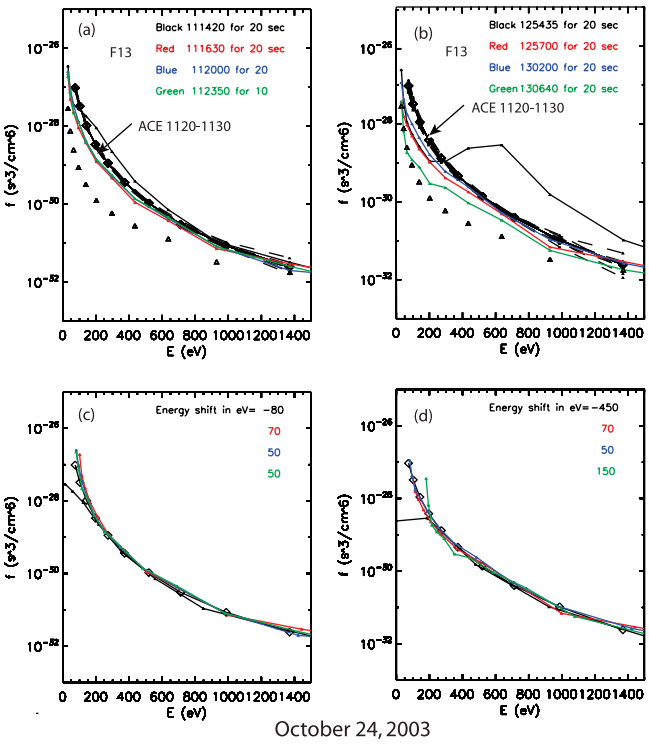

Figure 9. Distribution functions on two of the F13 passes shown in Figure 8. Note that the intense fluxes near the dusk boundary represented by thin black lines in Figures 9a and 9b agree well with ACE when shifted to the left, implying accelerating field-aligned potentials.

An additional increase in the 1.37 keV energy electrons near 1800 is conceivably associated with the 1549 event. Energy dispersion occurs, as can be seen most clearly by the increasingly later arrival of the peaks in f at the lower energies that are marked by x's in Figure 11a. Which type 3 event this dispersion is associated with is not clear due to the multiple events. The reason for the simultaneous increase at the several higher energies at 1730 (lack of energy dispersion) is not clear although *Gosling et al.* [2004b, 2004c] have noted how movements in the electron source regions and braiding of IMF field lines can produce such events.

[22] Figure 12 shows precipitating electrons during 4 northern hemisphere passes of various DMSP spacecraft that occurred between 1820 and 2010 UT on 10 June 2000. A clearly outward directed IMF dictates that solar burst electrons will precipitate in the northern hemisphere. F13 data in Figure 12a show normal polar rain but with a faint hint of electrons just above 4 keV. (The horizontal yellow line at 4 keV in these plots is to help the reader distinguish energy differences on the various passes.) A 5 keV electron will travel 1 AU in ~1 h so it is likely that these electrons observed ~80 min after 1656 type 3 onset and the accompanying flare are associated with this faint trace. On the next DMSP pass of F15 almost an hour later (1920), electrons are clearly seen up to almost 4 keV but there is a relative deficiency of electrons near 700 eV. This deficiency is reasonable since such electrons take at least 2.6 h to travel 1 AU which is greater than the 1.8 h since the 1656 type 3 onset. Thirty minutes later F14 observed similar, slightly lower-energy electrons above a similar slightly lower-energy deficiency. Around 2000 UT when F13 again made a pass, the solar electrons associated with the event had begun to decrease. Two earlier DMSP passes near 1640 and 1740 (not shown) show no evidence of electrons greater than 2 keV which helps eliminate the 1527 and 1549 events as sources for the energetic DMSP electrons.

[23] In Figure 13 the four panels each show four DMSP phase space density plots where the traces have been shifted to make the energies below 800 eV agree with ACE. The times of the traces in Figure 13 can be determined from the bars and the associated energy shifts in Figure 12. The earliest pass shown in Figure 13a exhibits fairly good agreement between ACE and F13 below 1 keV; DMSP counts are at background levels for energies above 1500 eV except near 3 keV which corresponds to the faint trace of electrons in Figure 12. SWEPAM electrons for the time 1720–1725 have been used in Figure 13a in accord with the usual assumption of a time independent source and convection of the relevant field lines from ACE to Earth. Figure 13b shows data from the time soon after the arrival of the more energetic solar electrons in Figure 12b. Now the SWEPAM data are averaged from 1900 to 1910 to reflect the fact that fluxes change with time. Enhancements of the 712, 987 and 1370 eV SWEPAM energies channels probably are associated with one of the 2 earlier solar bursts because it is too early for such energies to have arrived from the 1656 event. Higher energies could have arrived from the 1656 event and this is particularly likely in view of the lack of such energies from the earlier events at earlier times as mentioned above. The reason for the unusually large disagreement between DMSP and ACE near 1000 eV is not clear but may well result from the importance of both time variations in the electron flux and convection of field lines. It is also possible these higher energies are more field-aligned than usual such that they do not fill the 9-degree-SWEPAM pitch angle bin. Averaging over the bin would lead to an artificially low value. The solar wind density is unusually low on this day (1–2/cc) which will reduce scattering by coulomb collisions and enhance field alignment. It should also be noted that the high DMSP values just above 2 keV create a bump-on-tail electron distribution function. Since only the most field-aligned solar wind electrons make it down to the polar cap, that bump translates into a field-aligned bump in the upstream solar wind electron distribution. Bumps-on-tails in reduced (integrated over all perpendicular velocities) electron distributions are responsible for producing Langmiur waves that in turn produce the type 3 radio bursts [e.g., *Lin*, 1985; *Ergun et al.*, 1998].

[24] To summarize the solar electron events, it appears that two or three type 3-associated solar electron bursts arrived at Earth near the same time. A low-energy burst originating near 1527 and/or 1549 was measured by ACE SWEPAM beginning near 1730. A later event beginning near 1656 produced electrons above the SWEPAM energy range that were detected by ACE EPAM and by the higher DMSP energies. As would be expected, solar electron bursts can be detected over Earth's polar caps in the same manner

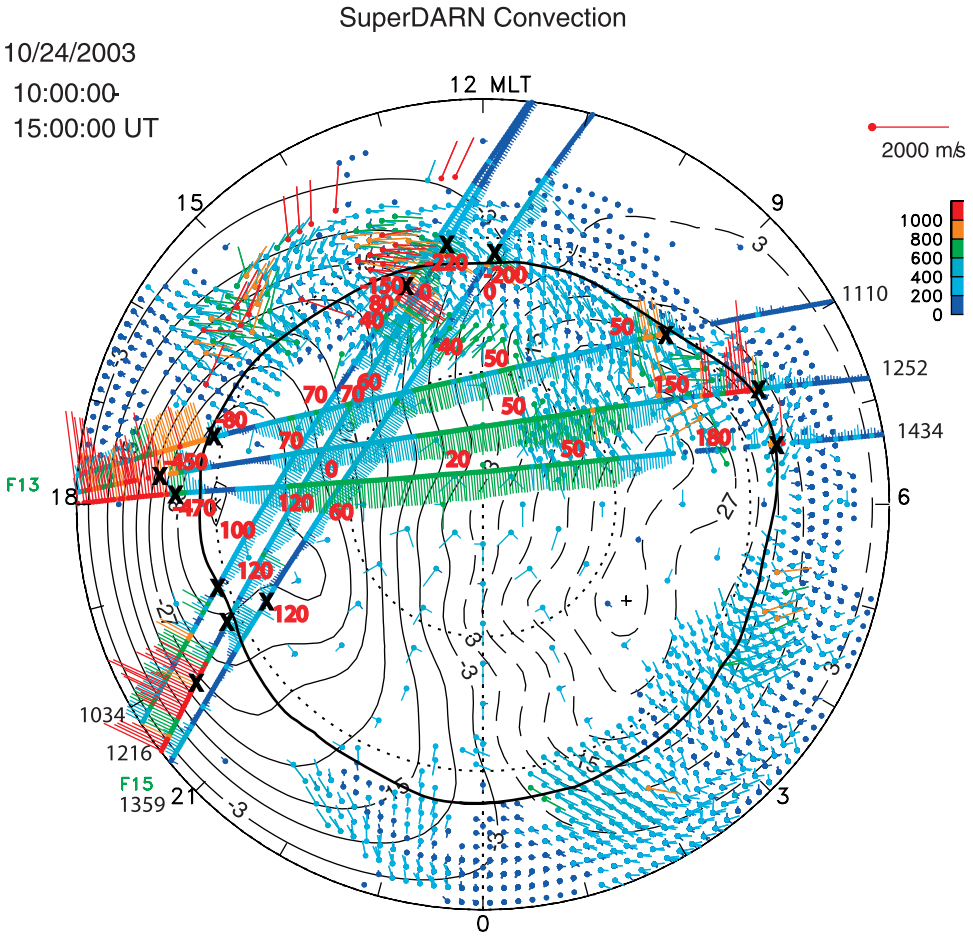

Figure 10. A view of the northern polar cap on 24 October 2003 in the same format as Figures 4 and 7. Negative potentials corresponding to accelerated electrons are seen near noon and near dusk.

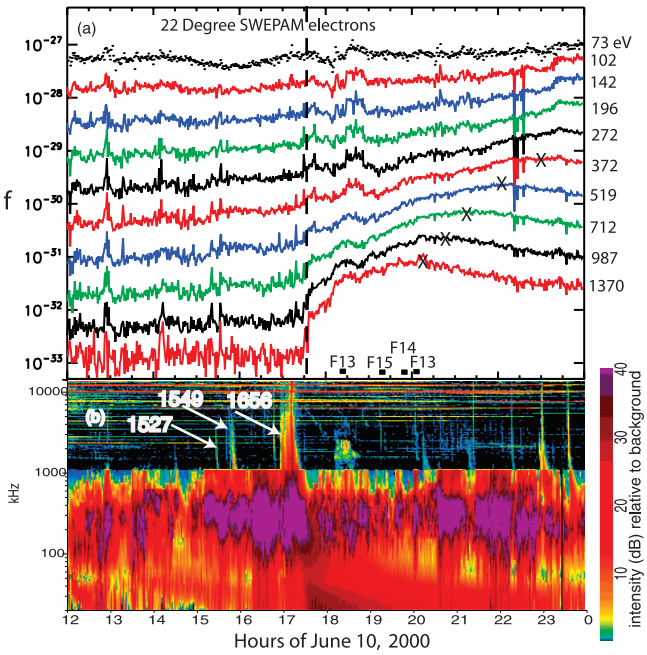

Figure 11. (a) ACE SWEPAM distribution functions at 22° pitch angle and various energies plotted versus time. (b) Wind waves data with white arrows denoting the three type 3 radio bursts associated with solar electron bursts detected by SWEPAM in the solar wind and DMSP over the polar cap. Bars mark the times of DMSP passes. Crosses mark the peaks at various energies that show energy dispersion following the 1549 type 3 onset.

as the solar wind strahl/heat flux electrons that produce polar rain.

5. Summary and Discussion

[25] To study cross-polar-cap gradients in the polar rain, the solar wind electrons measured by ACE have been compared to simultaneous measurements of precipitating electrons by DMSP spacecraft. Six days were investigated where the IMF was very southward in order to insure open polar cap field lines with smoothly varying polar rain. Electron distribution functions, f, from DMSP were averaged (usually for 20 s) at several locations across the polar cap in order to represent the polar cap gradient. Distribution functions of field-aligned (or anti-field-aligned) electrons at ACE were also averaged (usually over 10 min intervals) for comparison with DMSP in the appropriate hemisphere.

[26] When these simultaneous measurements were overlaid on f versus energy plots, generally good agreement was found, thus confirming the generally accepted idea that the solar wind heat flux or strahl is the source of polar rain. It was further noted, however, that the ACE f values usually exceeded those of DMSP but that shifting the DMSP trace in energy by amounts ranging from tens to a few hundred eV significantly improved the agreement with ACE. The simplest explanation of this fact is that a field-aligned potential existed between the interplanetary electron source and the arriving electrons at 835 km altitude. The fact that an increase in DMSP energy was usually required to obtain agreement implies that the entering electrons had been decelerated by an inward directed field-aligned E field.

[27] On individual DMSP passes, the most intense precipitation generally required the least energy shift. In the northern hemisphere the regions of most intense precipitation and least energy shift tended to occur on the dawn (dusk) sides for positive (negative) IMF B_y in the pattern first noted by *Meng et al.* [1977]. Everything reverses in the southern hemisphere as is commonly known for such polar cap phenomena. It was also clear that the nightside precipitation is less intense, as was found by *Gussenhoven et al.* [1984], requiring a larger DMSP energy shift to achieve agreement with ACE. The dawn/dusk gradient implies that the most intense precipitation tends to be associated with the smaller polar cap crescent convection cell more directly associated with the cusp and more recently opened field lines. The less intense precipitation with greater retarding potentials tends to be associated with the larger more circular cell with field lines that go further down the tail. It should also be noted that the deduced inward-directed field-aligned E fields will tend to retard outward moving ions.

[28] The most likely explanation for the deduced polar cap field-aligned potentials is based on an idea proposed by several workers [e.g., *Reiff et al.*, 1977; *Fairfield and Scudder*, 1985], developed quantitatively by *Wing et al.* [1996], extended in *Newell and Wing* [1998] and *Wing et al.* [2001] and summarized by *Wing et al.* [2005]; while field-aligned electrons follow the magnetic field lines into the magnetotail and polar cap, the more massive tailward moving magnetosheath ions are unable to do the same. To prevent a charge imbalance, a potential must be created to prevent enough low-energy electrons from entering the magnetosphere and traveling down to the polar cap and violating qusai-neutrality. *Wing et al.* [1996] added this potential to the ion entry model of *Onsager et al.* [1993] in order to better describe the entry of electrons. With the resulting model they were able to replicate with reasonable accuracy the entry of electrons to the LLBL, the cusp, the mantle and part of the dayside polar rain. A remaining problem in the model is the artificial capping of the potential at 250 eV that was necessary in order not to exclude all incoming electrons. The reason for this problem is most likely the omission of an ionosphere and resulting polar wind electrons in the model [*Wing et al.*, 2005]. The magnetic field model used in their original model limited results to field lines entering the tail earthward of X = −10 Re but later use of an improved magnetic field model [*Newell and Wing*, 1998; *Wing et al.*, 2001; see also *Wing et al.*, 2005] extended the results to X = −50 Re. The predicted potentials for the polar rain were found to be similar to those found above.

[29] In addition to the normal polar rain electrons, separate low-energy and high-energy solar electron bursts were identified in the solar wind by SWEPAM and EPAM data and in precipitating DMSP data. On the basis of transit times from Sun to Earth, it was argued that the more energetic DMSP electrons were associated with one type 3 radio burst while lower-energy electrons were more likely associated with an earlier burst. This precipitation of electrons from a solar electron burst is apparently the first report at energies below 10 keV that such electrons enter the

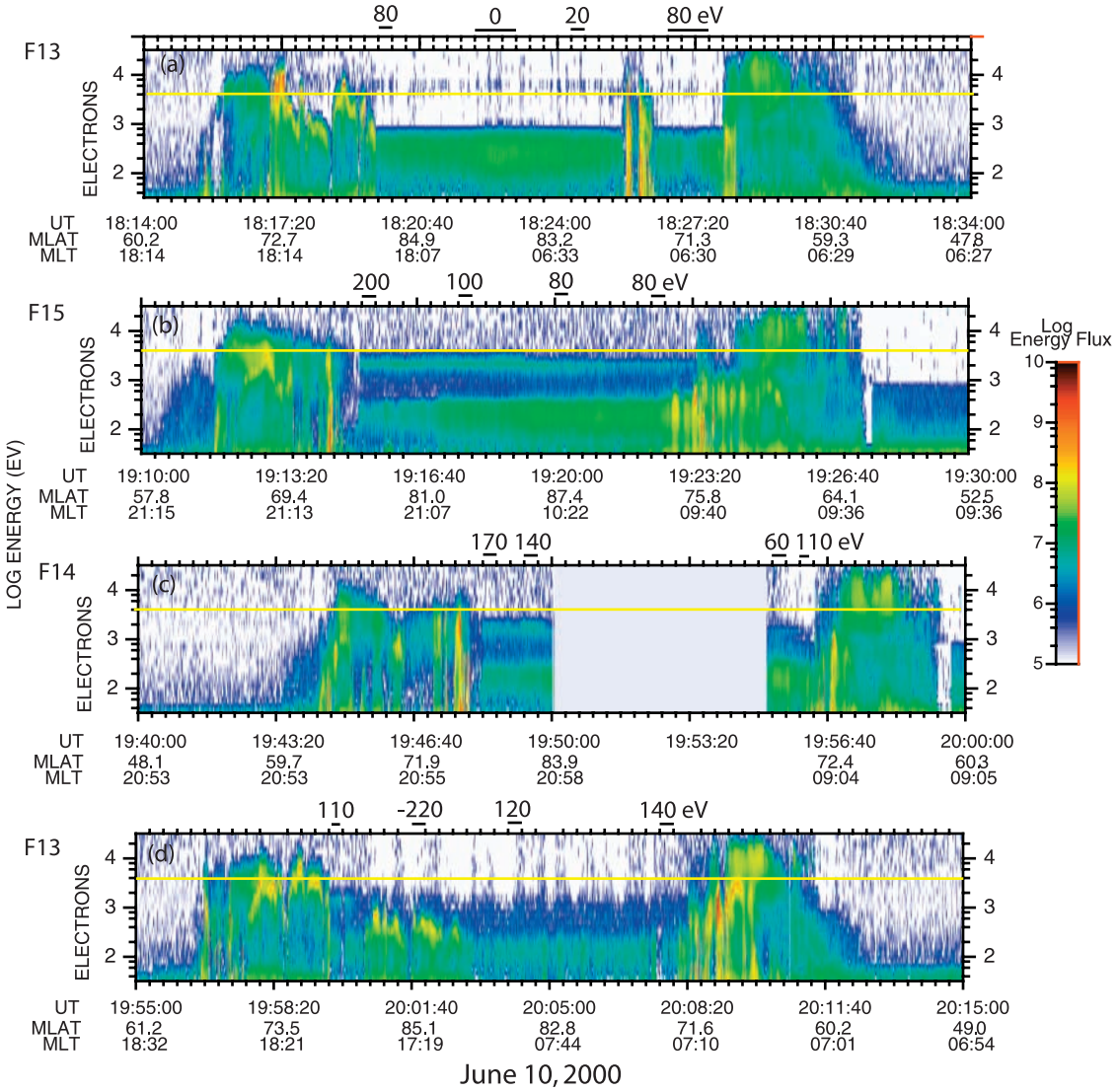

Figure 12. Four passes of the several DMSP spacecraft over the northern polar cap during the solar electron event on 10 June 2000.

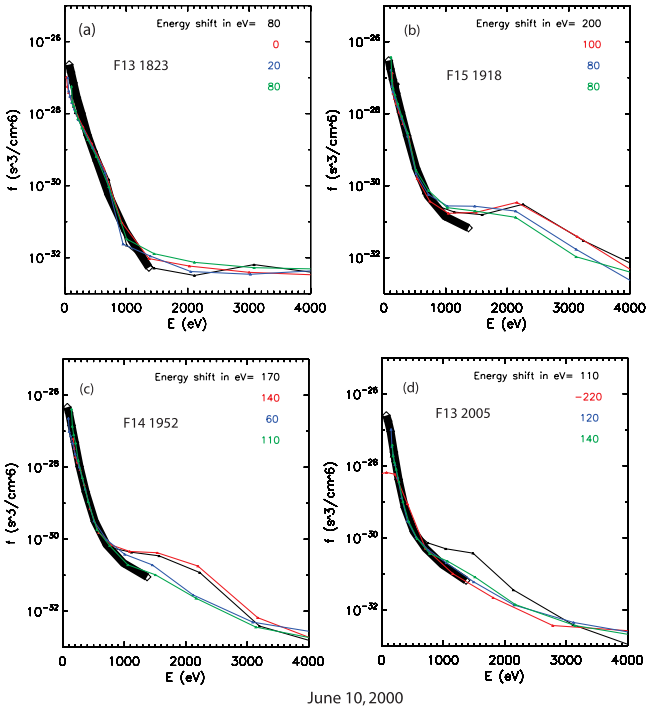

Figure 13. ACE and shifted DMSP electron distribution functions for the four passes in Figure 12. The unusual excesses in Figures 13b–13d at higher energies are due to the solar electron bursts. The flat portion of Figure 13b is due to the earliest arrival of higher energies and the resulting marginal bump-on-tail distribution may be that thought to lead to the type 3 radiation.

magnetotail and precipitate in the same manner as polar rain electrons.

[30] An additional feature found on a number of passes is the intense precipitation at the boundary of the polar cap as detected by F15 at 1822 in Figure 5. This intense precipitation can usually be made to agree with ACE by moving the DMSP values to lower-energy. Such a shift can be interpreted as an accelerating potential, but it may also be due to the fact that field lines near the cusp traverse the dayside magnetosheath where interplanetary densities have increased significantly on passing through the bow shock. Such higher densities may explain the more intense precipitation. (It is implicitly assumed that polar cap field lines leading to the more distant tail exit to the interplanetary medium where the bow shock is weak or non-existent.) A related example near the dusk polar cap boundary shows an enhanced precipitation intensity that seems to evolve gradually from the polar rain. This raises the question of whether or not this precipitation is accelerated polar rain on open field lines. If future work can resolve this question, the answer could lead to an improved understanding of the structure and dynamics of the magnetosphere.

[31] **Acknowledgments.** Work at LASP has been supported by NASA grant NNG05GJ55G. Work at Los Alamos was performed under the auspices of the U.S. Department of Energy, with financial support from the NASA ACE program. Operation of the SuperDARN radars is supported by the national funding agencies of the U.S., Canada, UK, France, Japan, South Africa, Italy, and Australia. J.M.R. acknowledges the support of NSF grant ATM-0418101 and S.W. acknowledges the support of NASA grant NNX06AB87G and NSF grants ATM-0703445 and ATM-0538513. We gratefully acknowledge the Center for Space Sciences at the University of Texas at Dallas and the U.S. Air Force for providing the DMSP thermal plasma data. M. L. Kaiser is thanked for useful discussions and for the preparation of the Wind Waves data. N. Gopalswamy helped in the interpretation of solar data.

[32] Zuyin Pu thanks George Siscoe for his assistance in evaluating this paper.

References

Anderson, P. C., D. L. McKenzie, D. W. Datlowe, J. D. Hawley, S. M. Petrinec, M. Schulz, and D. E. Larson (2000), Polar cap X-rays and electrons under low density solar wind conditions: Coordinated PIXIE and DMSP observations on 11 May 1999, *Geophys. Res. Lett.*, *27*, 4021, doi:10.1029/2000GL011983.

Baker, D. N., S. J. Bame, W. C. Feldman, J. T. Gosling, and R. D. Zwickl (1986), Strong electron bidirectional anisotropies in the distant tail: ISEE 3 observations of polar rain, *J. Geophys. Res.*, *91*, 5637, doi:10.1029/JA091iA05p05637.

Baker, D. N., S. J. Bame, J. T. Gosling, and M. S. Gussenhoven (1987), Observations of polar rain at low and high altitudes, *J. Geophys. Res.*, *92*, 13,547, doi:10.1029/JA092iA12p13547.

Chisham, G., et al. (2007), A decade of the Super Dual Auroral Radar Network (SuperDARN): Scientific achievements, new techniques and future directions, *Surv. Geophys.*, *28*, 33–109, doi:10.1007/s10712-007-9017-8.

Ergun, R. E., et al. (1998), Wind spacecraft observations of solar impulsive electron events associated with solar type III radio bursts, *Astrophys. J.*, *503*, 435, doi:10.1086/305954.

Fairfield, D. H., and J. D. Scudder (1985), Polar rain: Solar coronal electrons in the Earth's magnetosphere, *J. Geophys. Res.*, *90*, 4055.

Gopalswamy, N., S. Yashiro, M. L. Kaiser, R. A. Howard, and J.-L. Bougeret (2001), Radio signatures of coronal mass ejection interactions: Coronal mass ejection cannibalism?, *Ap. J.*, *548*, L91–L94, doi:10.1086/318939.

Gosling, J. T., D. N. Baker, S. J. Bame, and R. D. Zwickl (1986), Bidirectional solar wind electron heat flux and hemispherically symmetric polar rain, *J. Geophys. Res.*, *91*, 11,352, doi:10.1029/JA091iA10p11352.

Gosling, J. T., R. M. Skoug, and D. J. McComas (2003), Solar electron bursts at very low energies: Evidence for acceleration in the high corona?, *Geophys. Res. Lett.*, *30*(13), 1697, doi:10.1029/2003GL017079.

Gosling, J. T., R. M. Skoug, and D. J. McComas (2004a), Low-energy solar electron bursts and solar wind stream structure at 1 AU, *J. Geophys. Res.*, *109*, A04104, doi:10.1029/2003JA010309.

Gosling, J. T., C. A. de Koning, R. M. Skoug, J. T. Steinberg, and D. J. McComas (2004b), Dispersionless modulations in low-energy solar electron bursts and discontinuous changes in the solar wind electron strahl, *J. Geophys. Res.*, *109*, A05102, doi:10.1029/2003JA010338.

Gosling, J. T., R. M. Skoug, D. J. McComas, and J. E. Mazur (2004c), Correlated dispersionless structure in suprathermal electrons and solar energetic ions in the solar wind, *Astrophys. J.*, *614*, 412–419, doi:10.1086/423368.

Greenspan, M. E., C.-I. Meng, and D. H. Fairfield (1986), Simultaneous polar cap and magnetotail observations of intense polar rain, *J. Geophys. Res.*, *91*, 11,123, doi:10.1029/JA091iA10p11123.

Gussenhoven, M. S., D. A. Hardy, N. Heinemann, and R. K. Burkhardt (1984), Morphology of the polar rain, *J. Geophys. Res.*, *89*, 9785, doi:10.1029/JA089iA11p09785.

Lin, R. P. (1985), Energetic solar electrons in the interplanetary medium, *Sol. Phys.*, *100*, 537, doi:10.1007/BF00158444.

Lin, R. P., and K. A. Anderson (1966), Evidence for connection of geomagnetic field lines to the interplanetary field, *J. Geophys. Res.*, *71*, 4213.

McComas, D. J., S. J. Bame, P. Barker, W. C. Feldman, J. L. Phillips, P. Riley, and J. W. Griffee (1998), Solar wind electron proton alpha monitor (SWEPAM) for the Advanced Composition Explorer, *Space Sci. Rev.*, *86*, 563, doi:10.1023/A:1005040232597.

Meng, C.-I., S.-I. Akasofu, and K. A. Anderson (1977), Dawn-Dusk gradient of the precipitation of low-energy electrons over the polar cap and its relation to the interplanetary magnetic field, *J. Geophys. Res.*, *82*, 5271, doi:10.1029/JA082i032p05271.

Newell, P. T., and S. Wing (1998), Entry of solar wind plasma into the magnetosphere: Observations encounter simulation, in *Geospace Mass and Energy Flow: Results From the International Solar-Terrestrial Physics Program*, *Geophys. Monogr. Ser.*, vol. 104, edited by L. Horwitz, D. L. Gallagher, and W. K. Peterson, 73 pp., AGU, Washington, D. C.

Newell, P. T., S. Wing, C.-I. Meng, and V. Sigillito (1991a), The auroral oval position, structure, and intensity of precipitation from 1984 onward: An automated on-line data base, *J. Geophys. Res.*, *96*, 5877, doi:10.1029/90JA02450.

Newell, P. T., W. J. Burke, E. R. Sanchez, C.-I. Meng, M. E. Greenspan, and C. R. Clauer (1991b), The low-latitude boundary layer and the boundary plasma sheet at low altitude: Prenoon precipitation regions and convection reversal boundaries, *J. Geophys. Res.*, *96*, 21,013, doi:10.1029/91JA01818.

Newell, P. T., W. J. Burke, C.-I. Meng, E. R. Sanchez, and M. E. Greenspan (1991c), Identification of the plasma mantle at low altitude, *J. Geophys. Res.*, *96*, 35, doi:10.1029/90JA01760.

Ogilvie, K. W., R. Fitzenreiter, and M. Desch (2000), Electrons in the low density solar wind, *J. Geophys. Res.*, *105*, 27,277, doi:10.1029/2000JA000131.

Onsager, T. E., C. A. Kletzing, J. B. Austin, and H. MacKiernan (1993), Model of magnetosheath plasma in the magnetosphere: Cusp and mantle particles at low-altitudes, *Geophys. Res. Lett.*, *20*, 479, doi:10.1029/93GL00596.

Pagel, C., S. P. Gary, C. A. de Koning, R. M. Skoug, and J. T. Steinberg (2007), Scattering of suprathermal electrons in the solar wind: ACE observations, *J. Geophys. Res.*, *112*, A04103, doi:10.1029/2006JA011967.

Reiff, P. H., T. W. Hill, and J. L. Burch (1977), Solar wind plasma injection at the dayside magnetospheric cusp, *J. Geophys. Res.*, *82*, 479–491, doi:10.1029/JA082i004p00479.

Rich, F. J., and M. Hairston (1994), Large-scale convection patterns observed by DMSP, *J. Geophys. Res.*, *99*, 3827, doi:10.1029/93JA03296.

Ruohoniemi, J. M., and K. B. Baker (1998), Large-scale imaging of high-latitude convection with SuperDARN HF radar observations, *J. Geophys. Res.*, *103*, 20,797, doi:10.1029/98JA01288.

Shepherd, S. G., and J. M. Ruohoniemi (2000), Electrostatic potential patterns in the high latitude ionosphere constrained by SuperDARN measurements, *J. Geophys. Res.*, *105*, 23,005, doi:10.1029/2000JA000171.

Shirai, H., K. Maezawa, M. Fujimoto, T. Mukai, T. Yamamoto, Y. Saito, and S. Kokubun (1998), Entry process of low-energy electrons into the magnetosphere along open field lines: Polar rain electrons as field line tracers, *J. Geophys. Res.*, *103*, 4379, doi:10.1029/97JA02031.

Smith, C. W., J. L'Heureux, N. F. Ness, M. H. Acuna, L. F. Burlaga, and J. Scheifele (1998), The ACE magnetic fields experiment, *Space Sci. Rev.*, *86*, 613, doi:10.1023/A:1005092216668.

Wang, L., R. P. Lin, S. Krucker, and J. T. Gosling (2006), Evidence for double injections in scatter-free solar impulsive electron events, *Geophys. Res. Lett.*, *33*, L03106, doi:10.1029/2005GL024434.

Wing, S., P. T. Newell, and T. G. Onsager (1996), Modeling the entry of magnetosheath electrons into the dayside ionosphere, *J. Geophys. Res.*, *101*, 13,155, doi:10.1029/96JA00395.

Wing, S., P. T. Newell, and J. M. Ruohoniemi (2001), Double cusp: Model prediction and Observational Verification, *J. Geophys. Res.*, *106*, 25,571, doi:10.1029/2000JA000402.

Wing, S., P. T. Newell, and C.-I. Meng (2005), Cusp modeling and observations at low altitude, *Surv. Geophys.*, *26*, 341, doi:10.1007/s10712-005-1886-0.

Winningham, J. D., and W. J. Heikkila (1974), Polar cap auroral electron fluxes observe with Isis 1, *J. Geophys. Res.*, *79*, 949, doi:10.1029/JA079i007p00949.

D. H. Fairfield, Space Weather Laboratory, NASA Goddard Space Flight Center, Greenbelt, MD 20771, USA.

J. T. Gosling, Laboratory for Atmospheric and Space Physics, University of Colorado, 1234 Innovation Drive, Boulder, CO 80303, USA.

P. T. Newell and S. Wing, Johns Hopkins University Applied Physics Laboratory, Laurel, MD 20723, USA.

J. M. Ruohoniemi, Bradley Department of Electrical and Computer Engineering, Virginia Polytechnic and State University, 302 Whittemore Hall, Blacksburg, VA 24061, USA. (mikeruo@vt.edu)

R. M. Skoug, Los Alamos National Laboratory, P.O. Box 1663, Los Alamos, NM 87545, USA.